Environmental Earth Sciences (2019) 78:336
https://doi.org/10.1007/s12665-019-8291-3

ORIGINAL ARTICLE

The role of porewater exchange as a driver of CO_2 flux to the atmosphere in a temperate estuary (Squamish, Canada)

Rowena M. Diggle[1] · Douglas R. Tait[1,2] · Damien T. Maher[1,2] · Xander Huggins[3] · Isaac R. Santos[1]

Received: 15 July 2018 / Accepted: 25 April 2019 / Published online: 28 May 2019

Abstract

Porewater exchange is an important yet poorly understood component of the coastal carbon cycle. Here, a high-resolution automated radon (^{222}Rn, a natural porewater tracer) and CO_2 time series was conducted in the Squamish Central Estuary (Canada) over eight consecutive tidal cycles to assess the relative importance of porewater exchange on estuarine carbon dynamics. Radon and CO_2 observations revealed a clear tidal trend which is indicative of porewater exchange driven by tidal pumping. A radon mass balance indicated an average porewater exchange rate of 14.9 cm day^{-1} (4.3% of the tidal prism). The estuary was a net source of CO_2 to the atmosphere (average 212 ± 19 mmol m^{-2} day^{-1}). Porewater exchange accounted for 9%, 5% and 30% of net dissolved organic carbon (DOC), dissolved inorganic carbon (DIC) and CO_2 exported out of the Squamish Central Estuary, respectively, while porewater inputs of free CO_2 accounted for 38% of the atmospheric evasion. These flux estimates as well as strong correlations between pCO_2 and ^{222}Rn suggest that porewater exchange has a strong influence on CO_2 concentrations in the estuary even though they are a small contributor to overall DIC fluxes.

Keywords Submarine groundwater discharge · Greenhouse gases · Wetlands · Permeable sediments

Introduction

Although occupying a relatively small area, estuaries are biogeochemical hotspots and are often sources of CO_2 emissions to the atmosphere; largely due to elevated levels of biological production, remineralization and allocthonous organic matter inputs (Borges 2005; Chen et al. 2013; Jiang et al. 2008; Weston et al. 2014). The global estuarine CO_2 efflux is estimated to be 0.25 Pg C year^{-1}, roughly equal to CO_2 uptake from continental shelves (Cai 2011). However, large uncertainties still remain around estuarine flux estimates (±0.25 Pg C year^{-1}) (Laruelle et al. 2010; Regnier et al. 2013) and closing this knowledge gap is essential in accurately quantifying the role of estuaries in global carbon budgets.

An important and often overlooked component of the carbon cycle in estuaries is the contribution of submarine groundwater discharge and/or porewater exchange which is described by Moore (2010) as any flow of water from sediments to the coastal ocean. This can include both fresh terrestrial groundwater or recirculated seawater (Sadat-Noori et al. 2016; Santos et al. 2012a). Porewater exchange can significantly alter estuarine biogeochemical cycling if concentrations of carbon, nutrients, contaminants, metals and pollutants in porewater are high relative to receiving waters (Burnett et al. 2006; Slomp and Van Cappellen 2004; Tait et al. 2017). Despite often being volumetrically small, porewaters can provide a direct pathway for dissolved constituents to enter surface waters which can enhance primary production (Slomp and Van Cappellen 2004) and CO_2 evasion to the atmosphere (Macklin et al. 2014; Sadat-Noori et al. 2015a). In coastal systems, tidal pumping can be a significant driver of water column porewater exchange (Burnett et al. 2006; Santos et al. 2012b). Tidal pumping is the process whereby the action of tides creates regular flushing of sediments, potentially delivering solute enriched porewater to surface waters. The extent to which porewaters contribute to the partial pressure of CO_2 (pCO_2), dissolved inorganic carbon (DIC) and

✉ Douglas R. Tait
douglas.tait@scu.au

[1] National Marine Science Centre, Southern Cross University, PO Box 4321, Coffs Harbour, NSW 2450, Australia

[2] Southern Cross Geoscience, Southern Cross University, Lismore, NSW 2480, Australia

[3] School of Engineering, University of Guelph, Guelph, ON N1G 2W1, Canada

dissolved organic carbon (DOC) in surface waters remains poorly quantified and is often ignored in coastal carbon budgets (Atkins et al. 2013; Borges and Abril 2011; Porubsky et al. 2014).

Quantifying porewater fluxes can be challenging due to the heterogeneous spatial and temporal nature of porewater exchange (Burnett et al. 2006; Eller et al. 2014). The use of natural geochemical tracers to determine groundwater fluxes may be an effective and relatively inexpensive method to gain insight into porewater processes in estuarine and coastal systems. Radon (^{222}Rn; half-life 3.84 days) has been used as an effective tracer of porewater seepage due to its natural enrichment in water that has been in contact with sediments and its conservative nature (Peterson et al. 2010). As part of the uranium decay chain, ^{222}Rn is an ideal natural tracer in tidal systems due to its short half-life being comparable to residence times of coastal surface waters. Further, radon-in-water monitoring systems provide in situ, high frequency, continuous and precise observations over multiple tidal cycles, leading to large data sets that capture temporal and/or spatial variability (Burnett et al. 2006).

Past studies of global estuarine systems have found that most estuaries are supersaturated with CO_2 relative to the atmosphere, with low-latitude estuaries often strong sources of CO_2 and mid- to high-latitude estuaries generally weak sources of CO_2 to the atmosphere (Cai 2011; Dinauer and Mucci 2017; Laruelle et al. 2010; Laruelle et al. 2015). However, the lack of data in major geographic regions, such as Canada, China, Russia and the Arctic, creates uncertainty in global estimates of CO_2 emissions (Cai 2011; Chen et al. 2013). Further, the variability of CO_2 fluxes over diurnal and tidal timescales remains poorly understood (Cai 2011; Maher et al. 2015). North American estuaries have the largest estuarine surface area globally (41%), yet data suggest that they have the lowest CO_2 flux per unit area of all continents (Chen et al. 2013). The paucity of data from Canadian estuaries suggests large uncertainties (Dinauer and Mucci 2017; Regnier et al. 2013). Despite estuaries like the Gulf of St. Lawrence in eastern Canada being one of the worlds most studied estuarine systems, they have been omitted from global CO_2 flux estimates in major global reviews of estuarine CO_2 fluxes (Borges 2005; Cai 2011; Jiang et al. 2008; Laruelle et al. 2010) due to the lack of published data on surface water pCO_2.

We hypothesize that porewater exchange influences estuarine CO_2 emissions and contributes to the export of DIC and DOC to coastal waters. To investigate this hypothesis, measurements of dissolved and atmospheric carbon parameters were coupled with continuous in situ ^{222}Rn observations over multiple tidal cycles in a temperate Canadian estuary (Squamish Central Estuary). This enabled the investigation of the porewater drivers of CO_2 cycling over diurnal and tidal cycles and a ^{222}Rn mass balance allowing for the quantification of porewater exchange and related dissolved carbon inputs to the estuary.

Methods

Site description

To assess the influence of porewater exchange on CO_2 emissions to the atmosphere over tidal and diurnal cycles in a temperate estuary, a 5-day time series was conducted in the Squamish Central Estuary, Canada. Squamish Central Estuary is situated at the head of Howe Sound fjord in south western British Columbia (49°41′12″N, 123°10′42″W) (Fig. 1). The estuary has undergone significant transformation in the past 50 years, due mainly to urban and port developments. Howe Sound, the southernmost fjord in British Columbia, is 42 km long and connects the Squamish Central Estuary to the Salish Sea. Although the estuary is now separated from the Squamish River by a dyke, it is subject to tidal inundation from Howe Sound fjord and intermittent flow from a series of manmade culverts connecting the river and estuary. Temperatures during the summer (when this study took place) average 15.5 to 17.8 °C (June to August), while average winter temperatures range from 2.5 to 4.6 °C (November to January) (Government of Canada 2016). The average monthly precipitation is highest in winter months (316 mm) and lowest in summer months (69 mm) (Government of Canada 2016). The estuarine substrate consists of fine silts and sands, which are exposed for 1–2 h during low tide before being covered by 1–3 m of water at high tide.

Time series observations

Surface water observations were conducted at the time series station located approximately 1 km upstream from the estuary mouth (Fig. 1). A calibrated multiparameter sonde (Hydrolab DS5) was used to measure water column salinity, pH, temperature, dissolved oxygen (DO) saturation and turbidity at 15-min intervals. A current meter (SonTek Argonaut) was deployed in the middle of the estuary to monitor current velocity and direction of flow with data averaged over 10-min intervals. Windspeed data were acquired from an airport weather station located ~ 1 km north of the survey site. Salinity, temperature, DO saturation and pH within the culverts were measured with a calibrated multiprobe (HACH HQ40D).

To determine water column ^{222}Rn concentrations, surface waters were pumped continuously from a depth of ~ 0.5 m into a gas equilibrium device (GED) at a rate of ~ 3 L min^{-1}. The headspace of the GED was then sampled in a closed loop with a desiccant, a radon in-air monitoring device, modified for radon in-water (RAD7, Durridge) (Burnett

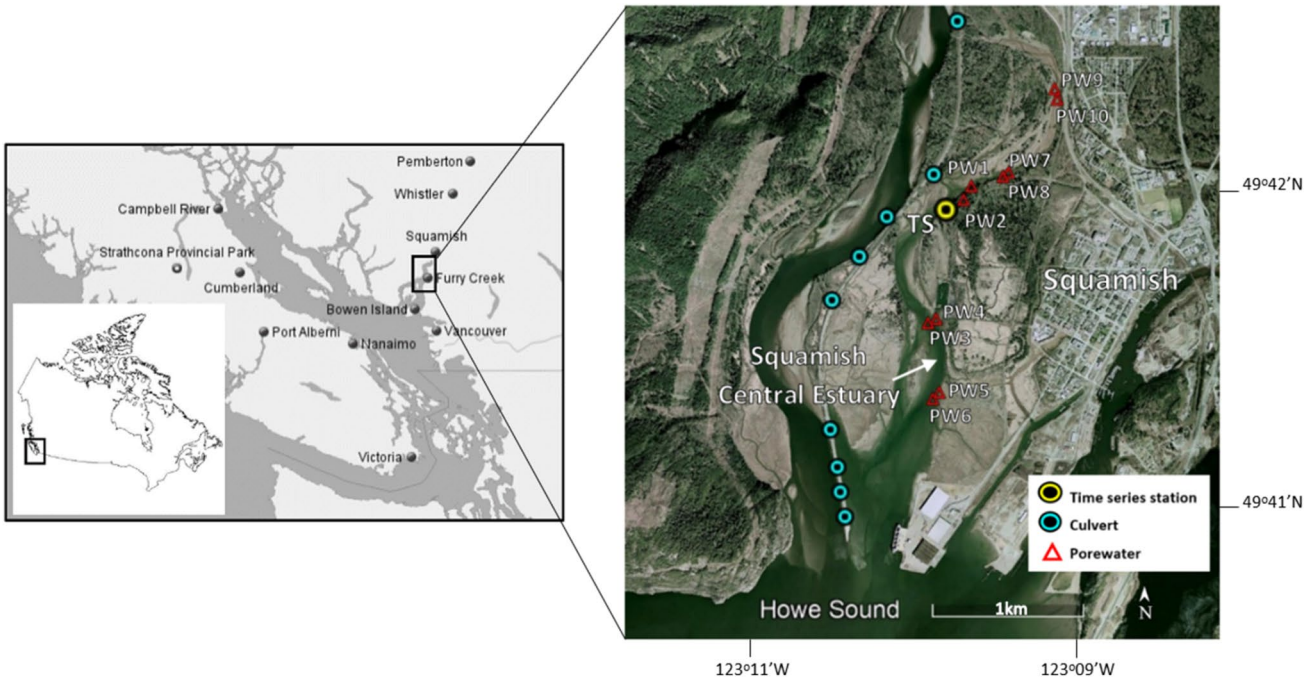

Fig. 1 Map of the Squamish Central Estuary (British Columbia, Canada) study site showing the location of the surface water time series station, porewater sample sites and the locations of culverts which connect the Squamish River and the Squamish Central Estuary at high tide

et al. 2010; Dulaiova et al. 2005) and a non-dispersive infrared-analyser (LiCor 7000) to determine CO_2 concentrations. The silicon semi-conductor within the ^{222}Rn monitor enables a count of positively charged ^{218}Po and ^{214}Po daughters, which are then used to derive ^{222}Rn concentrations from the temperature and salinity function of solubility (Schubert et al. 2012). Carbon dioxide concentrations were measured from the same headspace gas and converted to in situ pCO_2 using the temperature- and salinity-dependent solubility coefficients of Weiss (1974), correcting for the removal of water vapour from the measurement stream (Weiss and Price 1980) as described by Pierrot et al. (2009). The gas detectors were continuously run with data averaged over 30-min measurement intervals for ^{222}Rn and one-minute measurement intervals for CO_2. When water levels were too low (< 0.5 m) for pumping estuary water, an interpolation was applied to the ^{222}Rn and pCO_2 data. The interpolation used the first four data points either side of the missing data gap to apply a best fit six order polynomial. Radon and pCO_2 concentrations were measured in a culvert connecting the adjacent Squamish River to the estuary over the period where the two were connected during one tidal cycle (~ 5 h).

Discrete samples of DIC and DOC were taken at every low- and high-tide throughout the 5-day sampling period and every 2 h over a 24-h period on the 17th and 18th June, 2016. Samples were filtered through 0.7-µm filters (Whatman GF/F), treated with a saturated $HgCl_2$ solution and refrigerated before analysis using the wet oxidation method (St-Jean 2003) with an OI Aurora 1030 W interfaced with an Isotope Ratio Mass Spectrometer (Therma Delta V +) (St-Jean 2003).

Porewater measurements

Ten shallow bores of approximately one meter in depth were dug along the estuarine intertidal flats using a hand-held auger at low tide. This prevented any mixing of surface water with porewater during collection. The wells were purged three times before samples were drawn from the bores using a peristaltic pump. A calibrated multiprobe (HACH HQ40D) was used to measure pH, salinity, temperature and DO from each well. Porewater sampling for ^{222}Rn and CO_2 was conducted by firstly filling a 250-mL glass tight bottle with porewater three times to overflow before capping. A closed loop gas system (Durridge H_2O) in line with an RAD7 and Licor 7000 was then used to measure ^{222}Rn and CO_2 concentrations, respectively. Porewater DIC and DOC were sampled at each of the bores using a sample rinsed polypropylene syringe and filtered and analysed in the same manner as that for surface waters.

Calculations

A ^{222}Rn mass balance was used to quantitatively estimate porewater exchange by integrating the known ^{222}Rn sources (diffusion, radium-226 decay, river flow through

the culverts and incoming surface waters) and sinks (outgoing surface waters, atmospheric evasion and radioactive decay). The model incorporated incoming and outgoing temporal ^{222}Rn concentration measurements for each half hour time step over the eight complete tidal cycles (approximately 4 days) to estimate an integrated porewater exchange rate (PW; m^3 day^{-1}) (Tait et al. 2016):

$$PW = \frac{\left[\left(Rn_{wc}\Delta Wat_{vol}\right) - Ra_{Decay} - \left(Rn_{diff}A\right) - Rn_{culvert} + \left(J_{atm}A\right) + \left(Rn_{ave}\lambda Wat_{Vol}\right)\right]}{PW_{endmember}} \quad (1)$$

where Rn_{wc} is the sum of each average ^{222}Rn concentration at each 30 min time step (dpm m^{-3} day^{-1}; dpm is decays per minute); ΔWat_{Vol} is the change in volume of the overlying water (m^3); Ra_{decay} is the ^{222}Rn that is a result of ^{226}Ra decay (dpm day^{-1}); Rn_{diff} is the input of ^{222}Rn from sediment diffusion (dpm m^{-2} day^{-1}); $Rn_{culvert}$ is the ^{222}Rn input from the culvert (dpm day^{-1}), calculated by multiplying the culvert ^{222}Rn concentration by the water flux; A is the upstream inundated area (m^2); J_{atm} is the ^{222}Rn atmospheric evasion due to wind and current (dpm m^{-2} day^{-1}); Rn_{ave} is the average ^{222}Rn concentration over a tidal cycle, upstream and downstream; λ is the ^{222}Rn decay constant; and $PW_{endmember}$ is the ^{222}Rn average porewater concentration (dpm m^{-3}). Uncertainties were calculated based on standard propagation techniques similar to Sadat-Noori et al. (2015b).

The change in water volume (ΔWat_{Vol}) was estimated using a simple tidal prism approach which incorporates the change in depth multiplied by the estuary area. The surface area of the estuary upstream of the sample site was estimated by interpolating low- and high-tide estuary areas determined via aerial imagery. Discharge from the estuary was measured by multiplying current velocity by water column cross-sectional area for each time step and associated tide height, assuming a constant current velocity across the cross-sectional area. To incorporate the uncertainties associated with the assumption of uniform current velocities throughout the undulating estuary cross section, 20% uncertainties around current velocities were included in the propagation of errors techniques in mass balance calculations. As simultaneously measuring discharge through the 10 culverts draining into the estuary was not feasible, the difference in discharge volumes between the flood and ebb tides was attributed to culverts discharge. As this would attribute any fresh terrestrial groundwater inputs as culvert discharge, this may overestimate culvert inputs. However, as fresh terrestrial groundwater inputs have previously been shown to be only a minor proportion of overall porewater exchange in similar low relief intertidal flats (Sadat-Noori et al. 2016; Santos et al. 2014), fresh groundwater inputs were assumed to be negligible. Culvert discharge volumes were multiplied by the average culvert ^{222}Rn concentration for incorporation into the radon mass balance.

The diffusion of ^{222}Rn from sediments was determined by collecting ~ 1 L of sediment from locations in the upper, central and mouth of the estuary. The sediments were then incubated for 30 days in ~ 5 L of radium-free water before ^{222}Rn concentrations were measured in a closed loop system connected to a radon monitor (Lee and Kim 2006) and the average of the three locations used. To determine the amount of ^{222}Rn that is produced from the decay of radium (^{226}Ra), ~ 20 L of surface water was filtered through manganese (MnO_2) impregnated fibres and then analysed for ^{226}Ra via a delayed coincidence counter (Moore and Arnold 1996).

The estimation of atmospheric evasion of ^{222}Rn (J_{atm}) from both wind and current was calculated separately in 30-min time steps according to Burnett and Dulaiova (2003):

$$J_{atm} = k\left(C_{water} - \alpha C_{air}\right)A \quad (2)$$

where C_{water} and C_{air} are the concentrations of ^{222}Rn in water and air. A is the maximum area of the estuary; α is the Ostwald solubility coefficient of ^{222}Rn and k is the piston velocity at the air–water interface (m day^{-1}). An integration of wind, current and depth measurements Eq. (3) and Eq. (4) was then used to determine k (Wanninkhof 1992).

$$k_{wind} = 0.45\,\mu^{1.6}(Sc/600)^{-a} \quad (3)$$

where μ is the wind speed at a height of 10 m (m s^{-1}), Sc is the Schmidt number for radon, normalized to a Schmidt number of 600; and a is a variable power function dependent on wind speed and was set to 0.5 due to the non-smooth surface conditions. The piston velocity resulting from currents was calculated using (Borges et al. 2004):

$$k_{current} = 1.719w^{0.5}D^{-0.5}(Sc/600)^{-a} \quad (4)$$

where $k_{current}$ is the piston velocity resulting from current turbulence, w is the current speed (cm s^{-1}) and D is the water depth (m).

Carbon fluxes to the atmosphere and to the ocean

The atmospheric exchange of CO_2 was estimated using the calculations of Wanninkhof (1992):

$$CO_{2Flux} = k\alpha\left(C_{water} - C_{air}\right) \quad (5)$$

where C_{water} and C_{air} are the partial pressure of CO_2 (pCO_2 in μatm) in surface waters and in air, respectively; α is the solubility coefficient as a function of salinity and temperature using the constants of Weiss (1974) and k is the gas transfer velocity at the air–water interface (m day^{-1}). The

atmospheric concentration of CO_2 was assumed to be constant at 400 µatm.

The appropriate gas transfer velocity (k) is still widely debated because of limited measurements in estuaries (Jiang et al. 2008). Estimation of gas transfer rates in the open ocean is often calculated from wind speed; however, in estuaries, current velocity and bottom stress can be significant drivers of estuary turbulence and, therefore, gas exchange rates (Borges et al. 2004; Ho et al. 2016). For this study, we included a parameterization which takes into account current and bottom stress, adapted from Raymond and Cole (2001) and O'Connor and Dobbins (1956) and described by Ho et al. (2016):

$$k_{600} = 0.77v^{0.5}h^{-0.5} + 0.266\mu^2 \quad (6)$$

where k_{600} is the gas transfer velocity (normalized to a Schmidt number of 600), v is the current velocity (m s^{-1}), h is the depth and μ is the wind speed at a height of 10 m (m s^{-1}).

Estuarine import (flood tide) and export (ebb tide) of DIC and DOC were estimated for eight tidal cycles by multiplying 30-min discharge rates by the linear interpolation of carbon species concentration between high- and low-tide times. Total export and import rates over the eight cycles were then divided by the total number of days to calculate the daily average. The contribution of porewater exchange to fluxes of DOC, DIC and CO_2 was calculated as the percentage of porewater-derived flux in the net flux (outputs minus inputs). Free CO_2 was calculated using the solubility coefficient of CO_2 at a given temperature and salinity (Weiss 1974) and the measured pCO_2.

Results

Hydrological conditions

Conditions throughout the time series were predominantly dry, with patchy rainfall totalling 14 mm over the sampling period and 67 mm for the 30 days prior to sampling. Air temperatures during the week ranged from 4.7 to 22.9 °C and averaged 12.4 ± 4.1 °C. Low wind speeds were observed for most of the time series with short gusts of up to 4.5 m s^{-1}. The tidal trend remained constant during the 5 days of sampling with depths of ~ 0.4 m at low tide and ~ 2.8 m at high tide (Fig. 2). Surface water temperatures ranged from 11.6 to 20.2 °C, with an average of 14.0 ± 1.6 °C. Salinity remained low with an average of 2.1 ± 0.7 PSU and peaks of up to 5.3 PSU at the start of the incoming tide. The discharging volume of water out of the estuary during the ebb tide was ~ 1.6 times greater than the volume of water entering the estuary during the flood tide (Fig. 2), with the excess water assumed to be due to an inflow of water from the nearby culverts.

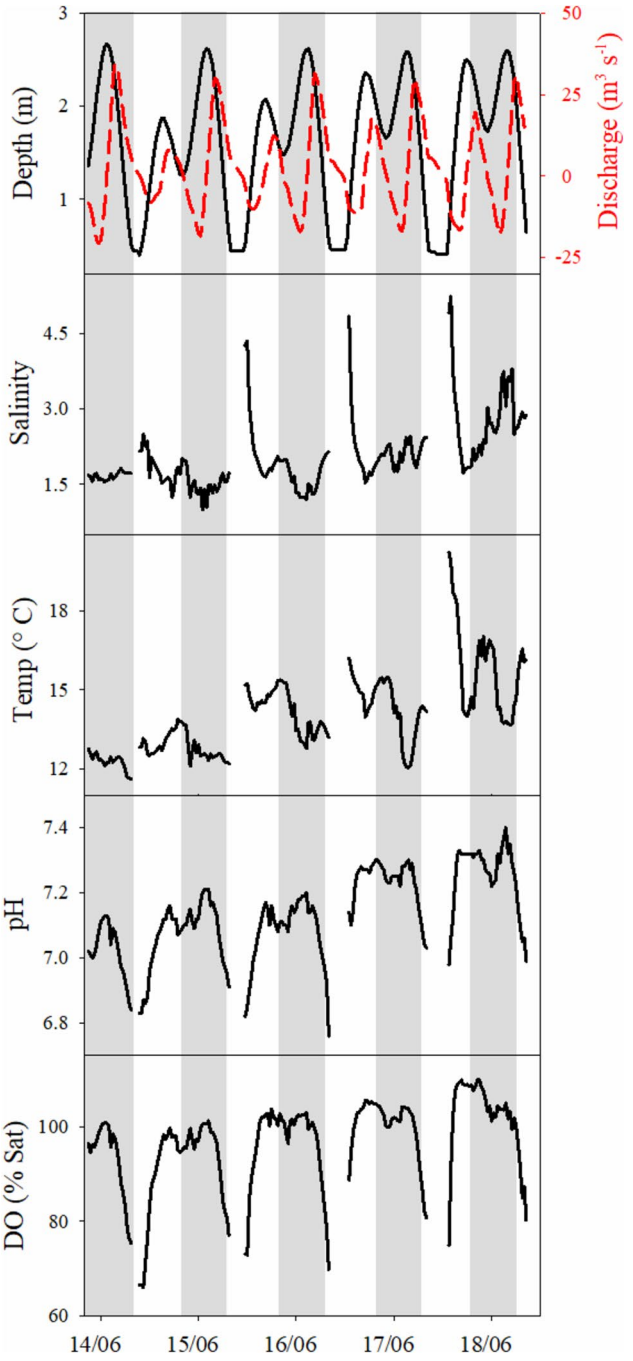

Fig. 2 Depth (m), discharge (m^3 s^{-1}) and physico-chemical observations during surface water time series of Squamish Central Estuary. Gaps in the data lines indicate periods of low water level. Shaded columns indicate night time

Surface water time series

A tidal trend was evident in DO saturation with the lowest saturation observed at low tide (min 66%) and highest saturation observed at high tide (max 108%) (Fig. 2). A similar tidal trend was observed for both DOC and DIC, with

the highest concentrations observed on low tide although the relationship is not entirely consistent (Fig. 3). Concentrations of DIC ranged from 335 µmol L^{-1} to 2181 µmol L^{-1} and DOC concentrations ranged from 26 µmol L^{-1} to 237 µmol L^{-1}, respectively. Both ^{222}Rn and pCO_2 displayed a similar tidal trend where the highest values were recorded at low tide and lowest at high tide (Fig. 3). Radon concentrations ranged from 4.0 dpm L^{-1} to 42.6 dpm L^{-1} and averaged 14.0 ± 1.0 dpm L^{-1} (including interpolated data). Surface water pCO_2 ranged from 720 to 10,527 µatm and averaged 3035 ± 162 µatm (including interpolated data) (Fig. 3). Maximum ^{222}Rn and pCO_2 values decreased over the 4 days of sampling which followed smaller tidal ranges during the smaller nighttime tide towards the end of the time series.

Significant correlations ($p < 0.05$) between pCO_2 and other variables were seen over the 4 day time series (Fig. 4). Salinity was weakly correlated with pCO_2 ($r^2 = 0.06$) with lower salinity during high tides. There was a significant negative correlation ($r^2 = 0.63$) with DO saturation and pCO_2 with lower DO saturation and higher pCO_2 at low tide. In contrast, there was a significant positive correlation between ^{222}Rn and pCO_2 values ($r^2 = 0.92$) with higher ^{222}Rn and pCO_2 at low tide. In all parameters beside salinity, there was a much greater range in values at low tide compared to high tide. There was a significant strong correlation between ^{222}Rn and depth ($r^2 = 0.83$) and ^{222}Rn and DIC ($r^2 = 0.84$) (Table 1). Further, there is also a strong correlation between DIC and both depth ($r^2 = 0.84$) and pCO_2 ($r^2 = 0.86$) with higher DIC concentrations at low tides. With the exception of DIC ($r^2 = 0.40$), salinity was decoupled from all the other variables.

Porewater and culvert observations

Porewater observations showed a high degree of spatial variability for all parameters (Table 2). Concentrations of ^{222}Rn in porewater ranged from 12.3 to 90.0 dpm L^{-1} with the lowest concentrations of ^{222}Rn located near the time series station. In the upper estuary porewater (PW9 and PW10), pCO_2 was almost fourfold higher than the highest value from all the other porewater sampling sites. There was a general trend of higher ^{222}Rn and pCO_2 values in samples collected further up in the intertidal zone (PW4, PW6, PW8 and PW10). The average porewater to average surface water ratio of all measured parameters ranged from a low of 0.4 (DO%) to 3.8 (pCO2) (Fig. 5). The average porewater pCO_2 and ^{222}Rn were much higher than surface waters (3.8 and 3.7 times, respectively). Concentrations of DIC in porewater followed a similar spatial trend to pCO_2 (Table 2), whereas DOC was highest at PW5 and PW6, located mid-way between the estuary mouth and time series station.

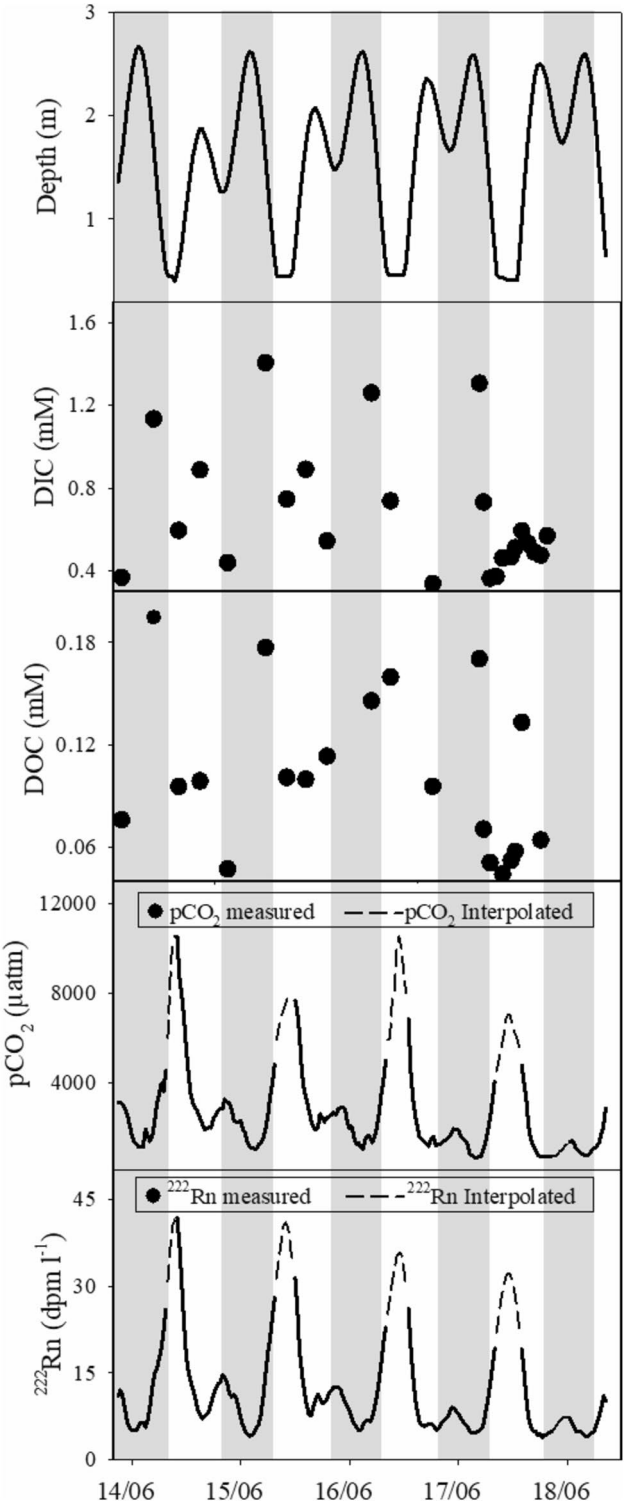

Fig. 3 Time series observations in surface waters sampled in the Squamish central estuary. Solid lines or symbols represent measured data. Dashed lines indicate interpolated data, with the missing data calculated using a best fit polynomial equation. Shaded columns indicate nighttime

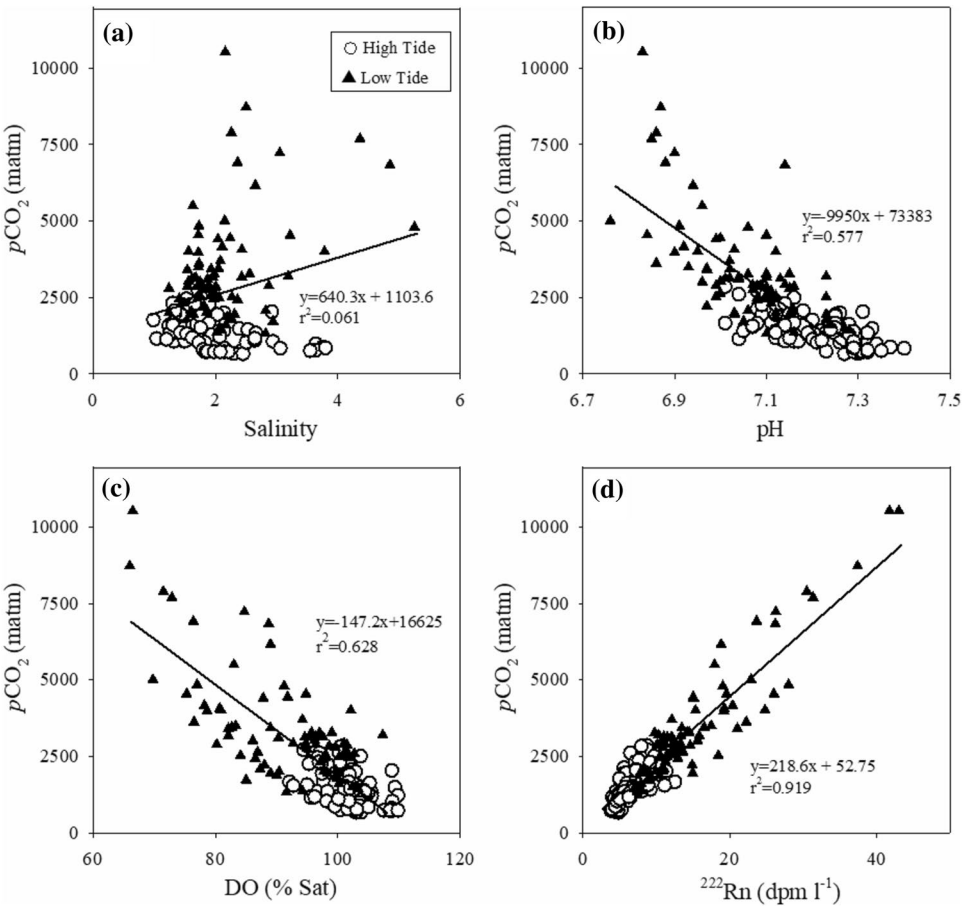

Fig. 4 Correlations between pCO_2 and salinity (**a**), pH (**b**), DO% saturation (**c**) and ^{222}Rn (**d**) in surface waters during time series 13/06/2016 to 18/06/2016 in the Squamish Central Estuary. Samples were delineated as either low tide or high tide based on water depths being either below or above the median tide height of 1.8 m

Table 1 Correlation coefficients (r^2) between measured parameters during the time series in the Squamish Central Estuary

	DIC	DOC	DO % sat	pCO_2	^{222}Rn	Depth	Salinity
DIC							
DOC	**0.59**						
DO% sat	**0.49**	0.25					
pCO_2	**0.86**	**0.46**	**0.63**				
^{222}Rn	**0.84**	**0.47**	**0.77**	**0.92**			
Depth	**0.84**	**0.38**	**0.66**	**0.65**	**0.83**		
Salinity	**0.40**	0.11	0.03	**0.06**	**0.08**	**0.10**	

Values highlighted in bold indicate significant relationships (p value ≤ 0.01)

Calculated from the estuary water balance, the average daily water flux from the culverts to the estuary was 2.1×10^5 m^3 day^{-1}. Multiplying the discharge by the average concentrations of the measured parameters showed that the culvert contributed an average of 3.1×10^4, 4.8×10^3 and 7.2×10^3 mol day^{-1} of DIC, CO_2 and DOC, respectively, and 1.4×10^9 dpm day^{-1} of ^{222}Rn to the estuary (Table 3).

Radon mass balance

A porewater exchange rate of 14.9 ± 3.1 cm day^{-1} was calculated from the radon mass balance model (Table 4). The largest source of ^{222}Rn to the system was provided by the incoming tide (67.2%), with the culvert also being a substantial source (32.6%). By far the largest sink of ^{222}Rn was the ebb tide (92.1%) with current-driven evasion (5.5%) being a much smaller sink followed by ^{222}Rn decay and wind-driven evasion contributing to a much lesser degree.

Carbon emissions and lateral export

During the time series, air–sea fluxes of CO_2 ranged from 13.5 mmol m^{-2} day^{-1} to 1315.2 mmol m^{-2} day^{-1} and averaged 212.0 ± 19 mmol m^{-2} day^{-1}. The flood tide was the

Table 2 Porewater observations for the Squamish central estuary

Sample ID	Latitude, longitude	Depth (m)	Salinity	DO (% sat)	pH	pCO_2		^{222}Rn (dpm L^{-1})	DIC (mM)	DOC (mM)
						(μatm)	(mM)			
PW1	49.706, 123.167	0.7	3.0	38.5	6.72	4404	0.21	21	1.24	0.12
PW2	49.706, 123.167	0.7	1.6	99.0	6.88	1988	0.08	12	0.62	0.04
PW3	49.692, 123.170	0.3	5.3	30.1	6.59	9431	0.40	70		
PW4	49.692, 123.170	1.0	7.0	23.2	6.96	10,091	0.41	90	2.88	0.28
PW5	49.698, 123.170	1.0	6.5	23.7	7.30	1769	0.07	31	2.59	0.41
PW6	49.698, 123.170	0.3	2.1	21.8	7.31	1972	0.08	55	0.93	0.32
PW7	49.707, 123.164	0.7	2.8	89.6	6.89	4391	0.18	27	1.32	0.11
PW8	49.707, 123.164	1.0	2.9	89.1	6.85	2880	0.11	63	0.86	0.08
PW9	49.712, 123.158	1.0	4.1	17.8	6.15	36,364	1.49	56	1.43	0.11
PW10	49.712, 123.158	1.1	3.5	20.7	5.90	39,629	1.67	85	1.95	0.18
	Average	0.8	3.9	42.7	6.76	11,292	0.47	51	1.54	0.18
	SE	0.1	0.6	11.3	0.15	4554	0.19	9	0.26	0.04

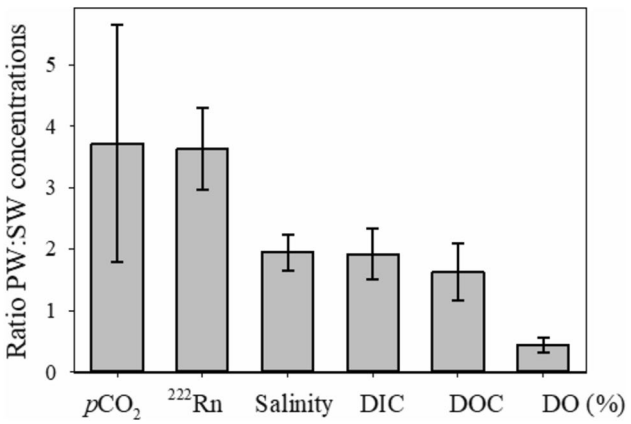

Fig. 5 Ratios of average porewater to surface water concentrations in measured parameters. Error bars were calculated using standard error propagation techniques

largest source of DOC, DIC and CO_2 to the estuary, contributing 78.1%, 85.1% and 80.6% of inputs, respectively (Table 5). The culvert was the second largest input for all carbon species. The estuary was a net exporter of DIC and DOC, with respective average net daily exports of 1.5×10^5 and 1.7×10^4 mol day^{-1} (Table 5); equivalent to 2693 and 305 mmol m^{-2} day^{-1}, respectively, if the estuary area is taken into account. Similar to the proportion of DIC in porewater (89%), the majority of carbon losses from the Squamish Central Estuary is via DIC (83%), followed by DOC (10%) and CO_2 evasion (7%) (Fig. 6).

Discussion

Porewater exchange

Coupled high-frequency measurements of ^{222}Rn and CO_2 showed that porewater exchange has a strong influence on pCO_2 concentrations in the estuary but they are a relatively small contributor to overall DIC fluxes. The Squamish Central Estuary porewater exchange rate of 14.9 ± 3.1 cm day^{-1} was within the range of previous estuarine studies. For example, Santos et al. (2014) calculated ^{222}Rn-derived porewater exchange rates of 27 ± 7 and 14 ± 6 cm day^{-1} in two New Zealand estuarine intertidal flats. Sadat-Noori et al. (2017) found porewater exchange rates between 13.6 and 27.8 cm day^{-1} using radium isotopes in a subtropical estuary with the higher exchange rates associated with the mangrove vegetation in the estuary. Burnett et al. (2006) calculated an average porewater rate of 12 ± 7 cm day^{-1} in a US tidal system. The porewater exchange in our study was equivalent to 4% of the average tidal prism volume (4.6×10^4 m^3), which was comparable to what was reported in the two New Zealand intertidal flats (12% and 6%) in the Santos et al.'s (2014) study.

Table 3 Average daily influxes of ^{222}Rn, carbon species and physico-chemical parameters from the culverts draining into the Squamish Central Estuary

	Discharge (m^3 day^{-1})	Salinity	DO (% Sat)	pH	^{222}Rn (dpm day^{-1})	DIC (mol day^{-1})	DOC (mol day^{-1})
Average	2.1×10^5	0.1	107.4	7.42	1.4×10^9	3.1×10^4	7.2×10^3
SE	(1.3×10^4)	(0.0)	(5.2)	(0.30)	(9.0×10^7)	(3.5×10^3)	(8.1×10^2)

Table 4 Radon sources and sinks forming the radon mass balance assessment for Squamish Central Estuary time series including the corresponding terms for Eq. (1)

Parameter	^{222}Rn	Units	Mass balance term
Source			
Flood tide	$2.9\times10^{9}\pm3.8\times10^{8}$	dpm day^{-1}	$Rn_{we}\Delta Wat_{Vol}$
Culvert	$1.4\times10^{9}\pm9.0\times10^{7}$	dpm day^{-1}	$Rn_{culvert}$
Sediment diffusion	$8.1\times10^{6}\pm5.2\times10^{5}$	dpm day^{-1}	$Rn_{diff}A$
Radium decay	$3.9\times10^{5}\pm4.1\times10^{4}$	dpm day^{-1}	Ra_{decay}
Total	$4.3\times10^{9}\pm3.9\times10^{8}$	dpm day^{-1}	$Rn_{we}\Delta Wat_{Vol}$
Sink			
Ebb tide	$4.4\times10^{9}\pm2.9\times10^{8}$	dpm day^{-1}	J_{atm}
Current evasion	$2.6\times10^{8}\pm3.6\times10^{7}$	dpm day^{-1}	$Rn_{ave}\lambda Rn_{we}\Delta Wat_{Vol}$
^{222}Rn decay	$8.0\times10^{7}\pm5.2\times10^{5}$	dpm day^{-1}	
Wind evasion	$3.0\times10^{7}\pm1.9\times10^{7}$	dpm day^{-1}	J_{atm}
Total	$4.8\times10^{9}\pm2.9\times10^{8}$	dpm day^{-1}	$PW_{endmember}$
PW^{222}Rn	$5.0\times10^{8}\pm3.8\times10^{7}$	dpm day^{-1}	A
$PW_{endmember}$	$50{,}870\pm9180$	dpm	PW
PW over entire area	8336 ± 1504	m^{-3}	
Maximum area	56,060	m^{3} day^{-1}	
Total PW exchange	14.9 ± 3.1	m^{2}	

All values were integrated over ~ 4 days of observations

Table 5 Carbon fluxes in and out of the Squamish Central Estuary, Canada

	DOC flux (mol day^{-1})	DIC flux (mol day^{-1})	CO_2 evasion (mol day^{-1})
Inputs			
Flood tide	$3.1\times10^{4}\pm1.5\times10^{3}$	$2.3\times10^{5}\pm9.6\times10^{3}$	
Culvert	$7.2\times10^{3}\pm8.1\times10^{2}$	$3.1\times10^{4}\pm3.5\times10^{3}$	
Porewater	$1.5\times10^{3}\pm3.2\times10^{2}$	$1.2\times10^{4}\pm2.1\times10^{3}$	
Total	$4.0\times10^{4}\pm1.7\times10^{3}$	$2.7\times10^{5}\pm2.1\times10^{4}$	
Outputs			
Ebb tide	$5.7\times10^{4}\pm2.8\times10^{3}$	$4.3\times10^{5}\pm1.9\times10^{4}$	
CO_2 evasion	–	–	$1.2\times10^{4}\pm6.0\times10^{2}$
Total	$5.7\times10^{4}\pm2.8\times10^{3}$	$4.3\times10^{5}\pm1.9\times10^{4}$	
Net flux	$1.7\times10^{4}\pm1.8\times10^{3}$	$1.5\times10^{5}\pm2.5\times10^{4}$	$1.2\times10^{4}\pm6.0\times10^{2}$

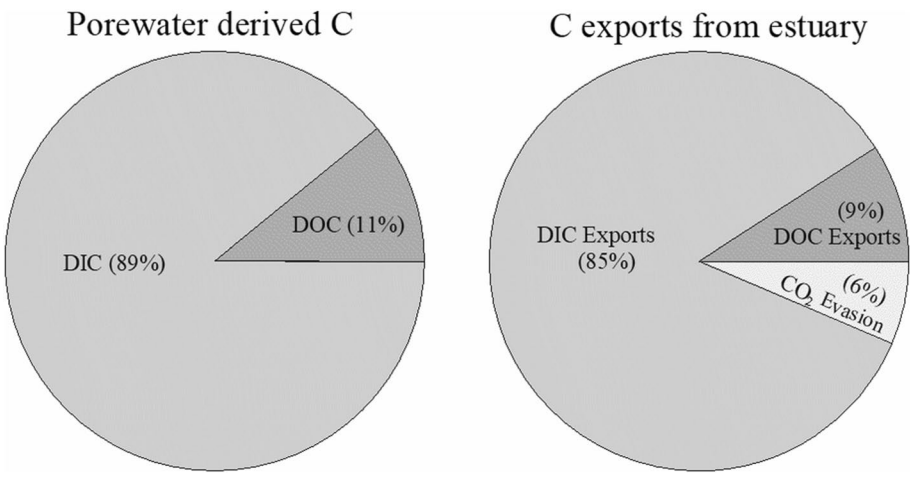

Fig. 6 The contribution of carbon species DIC, DOC, CO_2 and CO_2 evasion (losses) in porewater and losses from the Squamish Central Estuary

Drivers of porewater exchange can include pressure heads, tidal pumping and density inversions at the sediment–water interface (Santos et al. 2012a). These processes and interactions can influence porewater constituents, advection rates, residence times and the biogeochemical reactivity of the porewaters. Tidal pumping was assumed to be the main driver of porewater exchange in the estuary due to the strong correlation between tidal height and ^{222}Rn concentrations (Table 1). If fresh groundwater was entering in the upper parts of the estuary, a strong correlation between salinity and ^{222}Rn concentrations would have been expected despite only brackish waters (maximum salinity 5.2) entering the estuary from the Squamish River fed Howe Sound. However, the relationship was fairly weak ($r^2 = 0.08$).

The major contributor to the radon mass balance was ^{222}Rn inputs from the flood tide (61.3%), followed by the culvert (29.8%) and then porewater exchange (8.6%). Minor sources of radon to the system included sediment diffusion and radium decay, which accounted for less than 0.3% of sources and are in agreement with previous coastal groundwater studies (Peterson et al. 2010). Radon evasion was primarily driven by the ebb tide, with currents, wind and ^{222}Rn decay contributing a total of just 7.9%. While the estuary is not directly fed by Squamish River, it is indirectly connected through the series of culverts joining the two systems. This may create additional uncertainty due to variable water flow into the estuary and, therefore, provide a variable radon source which may affect the calculated discharge rate. Additional uncertainties also exist around ^{222}Rn concentrations during periods of low tide with ^{222}Rn concentrations interpolated for 18% of the time of the tidal cycles due to low water levels. However, this accounted for 6.5% of the tidal flows and as such is assumed to be a minor uncertainty of the mass balance.

An important component of uncertainty when estimating porewater exchange using a radon mass balance is deriving the porewater endmember (Dulaiova and Burnett 2008). Sadat-Noori et al. (2015b) showed that a porewater endmember sample size of > 12 can stabilize the standard error to < 30%. Here, we collected 10 porewater samples with ^{222}Rn concentrations ranging from 12.3 to 90.0 dpm L^{-1} and a standard error of ~ 17%. Our mass balance estimate of 14.9 ± 3.1 cm day^{-1} was calculated using the average $^{222}Rn_{endmember}$; however, if we used the highest concentration in porewater when constructing the radon mass balance, the porewater exchange rate would have been 8.1 cm day^{-1}, or if the lowest concentration was applied to the mass balance, the porewater exchange rate would be 59.0 cm day^{-1}.

Carbon dioxide dynamics

The Squamish Central Estuary was shown to be a source of CO_2 to the atmosphere with an average flux of 212 ± 19 mmol m^{-2} day^{-1} (77 mol C m^{-2} year^{-1}) and an average surface water pCO_2 of 3035 ± 162 µatm. There are limited data available for air–sea CO_2 fluxes in Canada. In the upper estuary of the St Lawrence River, Canada, an average pCO_2 of 571 ± 72 µatm was observed, with air–sea gas fluxes in the upper estuary ranging between 6.1 ± 3.0 mmol m^{-2} day^{-1} using Wanninkhof (1992) k values and 12.3 ± 5.4 mmol m^{-2} day^{-1} using Raymond and Cole (2001) k values (Dinauer and Mucci 2017). In contrast, in the partially ice-covered Canada Basin (77–80 °N), pCO_2 ranged from 250 to 368 µatm and seawater was found to be a net sink of atmospheric CO_2 (6.5 ± 1.3 Tg year^{-1}) (Sun et al. 2017). The CO_2 flux of 212 mmol m^{-2} day^{-1} and surface water pCO_2 of 3035 µatm observed for Squamish Central Estuary are comparable to the global average of upper estuary fluxes calculated by Chen et al. (2013) of 188 ± 70 mmol m^{-2} day^{-1} and average pCO_2 of 3033 ± 1078 µatm. Sampling was not possible during the lowest part of the tidal cycle and interpolated data were not used to calculate the air–sea fluxes. Hence the estimates are considered conservative.

A significant uncertainty when estimating air–sea gas exchanges results from the gas transfer parameterization (k) (Ho et al. 2016). Wind speed, current velocity and depth are major forces driving turbulence and, therefore, CO_2 evasion at the water–air interface in shallow estuaries (Borges and Abril 2011; Borges et al. 2004; Ho et al. 2016). The parameterization by Ho et al. (2016) is an adaptation of O'Connor and Dobbins (O'Connor and Dobbins 1956) which takes into account bottom-generated shear and wind stress. Observed and modelled data in a study in the Shark River, Florida found that replacing the coefficient of 1.539 in O'Connor and Dobbins (1956) to 0.77 was a better fit in a tidal estuary (Ho et al. 2016). O'Connor and Dobbins (1956) parameterization is based on reaeration coefficients in streams and does not include wind stress, while the Ho et al. (2016) parameterization incorporates wind-generated turbulence. As such, we believe that the parameterization developed by Ho et al. (2016) best fits the Squamish Central Estuary hydrology and physical conditions. However, it must be noted that the current velocities in the study were measured at only one location and then applied to the entire domain which would increase uncertainties around estimates.

Directly comparing different estuarine and river systems can be problematic due to the different hydrological and geographic settings, seasonality, different sampling methods, and the use of different models for calculating gas transfer velocities (Laruelle et al. 2010; Laruelle et al. 2015). Inner estuaries with similar topography and latitude to Squamish Central Estuary may provide the closest comparison. For example, a study by Ferrón et al. (2007) in a shallow mid-latitude estuarine salt marsh system had a pCO_2 range of 981–4680 µatm and a CO_2 atmospheric flux range of 73 to

177 mmol m^{-2} day^{-1}. The Duplin River in Georgia, USA (31.5 °N) is also a marsh-dominated tidal estuary and has been reported to have a pCO_2 range of 500–3000 µatm and an annual average CO_2 air–sea flux of 58.5 mmol m^{-2} day^{-1} (Wang and Cai 2004). The lower annual average air–sea flux in Duplin River compared to Squamish Central Estuary may be due to greater uptake by marsh macrophytes and autotrophy in the Dulpin River (Wang et al. 2018). The study did not account for fluxes from sediments or exposed seagrass vegetation at low tide which can be a significant proportion of a carbon budget (Borges and Abril 2011) and as such may lead to an over estimation of the contribution of porewater to the total carbon pool.

Porewater as a driver of carbon dynamics

Carbon dioxide in estuaries has been suggested to be predominantly driven by the net heterotrophy of the system and direct input of CO_2 from upstream surface waters (Borges and Abril 2011). However, our study showed a tight coupling between pCO_2 and porewater exchange (^{222}Rn concentrations) (Fig. 4; $r^2 = 0.92$, $n = 217$, $p < 0.001$). Strong relationships have been found between ^{222}Rn and CO_2 fluxes in a range of coastal areas (Atkins et al. 2013; Jeffrey et al. 2016; Maher et al. 2015). In a coastal floodplain creek estuarine system, Atkins et al. (2013) found ^{222}Rn to be tidally driven, with a strong inverse relationship to depth ($r^2 = 0.71$, $p < 0.01$, $n = 157$) and porewaters were suggested to drive pCO_2 in the upper estuary ($r^2 = \sim 0.80$). A tidal trend was also found in Squamish Central Estuary, with significant correlations between depth and pCO_2 ($r^2 = 0.65$) and depth and ^{222}Rn ($r^2 = 0.83$). In stratified salt wedge estuaries, groundwater may also be an important driver of other more powerful greenhouses such as methane, with Tait et al. (2017) showing tight coupling of ^{222}Rn and methane in anaerobic bottom waters of an Australian estuary.

Variability in pCO_2 can be driven by changes in gas solubility driven by temperature, sediment water convection, wind speed and evasion rates and also biological production and respiration (Maher et al. 2015). A diurnal temperature effect can lead to higher pCO_2 during the day and lower pCO_2 at night; however, this study found that small peaks were also observed during night time and the largest peak in pCO_2 occurred in the morning before higher day time temperatures occurred. Biological activity in surface waters generally leads to lower pCO_2 during the day, driven by CO_2 uptake by primary producers and higher pCO_2 at night from in situ respiration. However, in this study, both DO and pCO_2 were more strongly controlled by tidal dynamics than diurnal oscillations in metabolism (Figs. 2, 3) If metabolism was the dominant driver of DO and pCO_2, DO would be expected to peak during the day and pCO_2 would peak during the night. Interestingly, supersaturation of both DO and pCO_2 was observed simultaneously, suggesting an external source of dissolved CO_2, most likely porewater exchange counteracting photosynthesis-driven CO_2 uptake.

There were distinct tidal trends in pCO_2, ^{222}Rn and DIC and DO saturation. The tidal trends in surface water pCO_2 may be driven by carbon inputs and mixing of fresh and saline water, porewaters enriched in CO_2, lateral inputs from vegetated areas and biological processes mediated by organic matter and/or nutrient input (Maher et al. 2015). Dissolved inorganic carbon and pCO_2 in estuarine surface waters are thought to be controlled by the breakdown of organic carbon by in situ microbial degradation and inorganic carbon laterally transported from adjoining conduits, such as rivers, wetlands and porewaters (Bauer et al. 2013). Here, the strong correlation between DIC and ^{222}Rn along with the calculated porewater DIC inputs suggests that porewater exchange is an important driver of DIC dynamics in the Squamish Central Estuary, as found in other systems (Maher et al. 2013; Porubsky et al. 2014; Sadat-Noori et al. 2015a; Wang et al. 2015). This is supported in our results where DIC showed strong correlations with ^{222}Rn, pCO_2 and depth (Table 3). The average DIC concentration of 802 ± 54 µmol L^{-1} was less than observations in the upper estuary of the St. Lawrence River, where the average DIC concentration was 1514 ± 242 µmol Kg^{-1} (Dinauer and Mucci 2017). In that study, temperature and DIC dynamics resulting from biological processes and water mixing were suggested to be the most important drivers of pCO_2 in surface waters.

In Squamish Central Estuary, the porewater-derived fluxes of DIC and DOC of 220 and 26 mmol m^{-2} day^{-1}, respectively, are similar to shallow DIC and DOC porewater fluxes in a subtropical estuary, Australia (Sadat-Noori et al. 2015a). In that same study, porewater-derived DIC fluxes were 213 ± 129 mmol m^{-2} day^{-1}; however, the DOC flux (183 ± 521 mmol m^{-2} day^{-1}) was much higher than that in our study. Porewater exchange accounted for 9%, 5% and 30% of net DOC, DIC and CO_2 exported out of the Squamish Central Estuary, respectively, and for 39% of the CO_2 atmospheric evasion. The relatively low contribution of porewater exchange-driven carbon flux to the overall exports is due to the large inputs of carbon from the series of culverts connecting the nearby Squamish River to the estuary. If the carbon inputs from the culverts are removed, then porewater exchange accounts for 15%, 6% and 43% of DOC, DIC and CO_2 exports from the estuary. Sadat-Noori et al. (2015a) used a multi-time series approach to show that groundwater-derived inputs of free CO_2 accounted for 54% of observed water to air fluxes in a subtropical estuary while in the Squamish Central Estuary porewater inputs of free CO_2 accounted for 38% of the atmospheric evasion.

Porewater exchange in estuaries has been shown to be highly temporally variable and it is, therefore, essential

in accurately quantifying estuarine carbon dynamics to design studies that incorporate multiple tidal cycles (Santos et al. 2014). Further, seasonal patterns of pCO_2 and DIC have been observed in estuaries along the Georgia Coast which were attributed to varying organic matter decomposition rates and changes in river discharge (Cai 2011; Jiang et al. 2008). A seasonal study of DOC and TOC export completed by Clair et al. (1999) of 32 Canadian rivers and estuaries found that in the south-western region of Canada, winter and fall had the largest exports which were driven by high levels of rainfall. Our study was completed in the summer months and, therefore, our estimates may be in the lower range for the Squamish region.

Implications and conclusion

This study addresses a major geographic knowledge gap in global CO_2 emissions from estuaries. With a fourfold difference in the range of CO_2 emissions in low-latitude estuaries (Laruelle et al. 2010), it is essential to incorporate as many of the major geographic coastal regions as possible, namely Canada, China, Russia, Africa and South America, which are underrepresented in global estimates (Cai 2011). This study showed that the temperate Squamish Central Estuary was a net source of CO_2 to the atmosphere and a net exporter of DIC and DOC.

This study also builds on the published literature by highlighting that porewater exchange can be an important driver of estuarine carbon dynamics. Previous major reviews of estuarine CO_2 degassing have failed to account for the role of porewater exchange in driving high CO_2 fluxes (Cai 2011; Dinauer and Mucci 2017; Laruelle et al. 2010; Laruelle et al. 2015). The clear tidal trend in ^{222}Rn observations during the time series shows that seawater recirculation (tidal pumping) may be an important driver of porewater exchange. As estuarine sediment can be a ready source of bioavailable carbon and provide ideal conditions for a range of biogeochemical cycling, understanding the exchange of water through sediments is essential to the greater understanding of estuarine carbon dynamics.

Acknowledgements We would like to thank Edith Trobe from the River Watershed Society for providing background on the estuary and input into the study design. Ceylena Holloway from NMSC provided equipment logistics and laboratory analysis. We acknowledge funding from the Australian Research Council (DE140101733, DE1500100581 and LE120100156) for analytical instrumentation and field investigations support. DRT also received support through an Australian Research Council DECRA Fellowship (DE180100535) during the data analysis and writing of the manuscript. The original data can be obtained from DRT.

References

Atkins ML, Santos IR, Ruiz-Halpern S, Maher DT (2013) Carbon dioxide dynamics driven by groundwater discharge in a coastal floodplain creek. J Hydrol 493:30–42

Bauer JE, Cai W-J, Raymond PA, Bianchi TS, Hopkinson CS, Regnier PA (2013) The changing carbon cycle of the coastal ocean. Nature 504:61–70

Borges AV (2005) Do we have enough pieces of the jigsaw to integrate CO2 fluxes in the coastal ocean? Estuaries 28:3–27

Borges AV, Abril G (2011) Carbon dioxide and methane dynamics in estuaries. Academic, Waltham

Borges AV, Vanderborght J-P, Schiettecatte L-S, Gazeau F, Ferrón-Smith S, Delille B, Frankignoulle M (2004) Variability of the gas transfer velocity of CO2 in a macrotidal estuary (the Scheldt). Estuaries 27:593–603

Burnett WC, Dulaiova H (2003) Estimating the dynamics of groundwater input into the coastal zone via continuous radon-222 measurements. J Environ Radioact 69:21–35

Burnett W, Aggarwal P, Aureli A, Bokuniewicz H, Cable J, Charette M, Kontar E, Krupa S, Kulkarni K, Loveless A (2006) Quantifying submarine groundwater discharge in the coastal zone via multiple methods. Sci Total Environ 367:498–543

Burnett WC, Peterson RN, Santos IR, Hicks RW (2010) Use of automated radon measurements for rapid assessment of groundwater flow into Florida streams. J Hydrol 380:298–304

Cai W-J (2011) Estuarine and coastal ocean carbon paradox: CO_2 sinks or sites of terrestrial carbon incineration? Ann Rev Mar Sci 3:123–145

Chen C-T, Huang T-H, Chen Y-C, Bai Y, He X, Kang Y (2013) Air–sea exchanges of CO_2 in the world's coastal seas. Biogeosciences 10:6509–6544

Clair T, Ehrman J, Higuchi K (1999) Changes in freshwater carbon exports from Canadian terrestrial basins to lakes and estuaries under a $2\times CO_2$ atmospheric scenario. Global Biogeochem Cycles 13:1091–1097

Dinauer A, Mucci A (2017) Spatial variability in surface-water pCO_2 and gas exchange in the world's largest semi-enclosed estuarine system: St. Lawrence Estuary (Canada). Biogeosciences 14:3221

Dulaiova H, Burnett WC (2008) Evaluation of the flushing rates of Apalachicola Bay, Florida via natural geochemical tracers. Mar Chem 109:395–408

Dulaiova H, Peterson R, Burnett W, Lane-Smith D (2005) A multi-detector continuous monitor for assessment of 222 Rn in the coastal ocean. J Radioanal Nucl Chem 263:361–363

Eller KT, Burnett WC, Fitzhugh LM, Chanton JP (2014) Radium sampling methods and residence times in St. Andrew Bay, Florida. Estuaries Coasts 37:94–103

Ferrón S, Ortega T, Gómez-Parra A, Forja J (2007) Seasonal study of dissolved CH_4, CO_2 and N_2O in a shallow tidal system of the bay of Cádiz (SW Spain). J Mar Syst 66:244–257

Government of Canada (2016) Weather, Climate and Hazards. Webpage: https://www.canada.ca/en/services/environment.html. Accessed: 9 Feb 2017

Ho DT, Coffineau N, Hickman B, Chow N, Koffman T, Schlosser P (2016) Influence of current velocity and wind speed on air-water gas exchange in a mangrove estuary. Geophys Res Lett 43:3813–3821

Jeffrey LC, Maher DT, Santos IR, McMahon A, Tait DR (2016) Groundwater, acid and carbon dioxide dynamics along a coastal wetland, lake and estuary continuum. Estuaries Coasts 39:1325–1344

Jiang L-Q, Cai W-J, Wang Y (2008) A comparative study of carbon dioxide degassing in river-and marine-dominated estuaries. Limnol Oceanogr 53:2603–2615

Laruelle GG, Dürr HH, Slomp CP, Borges AV (2010) Evaluation of sinks and sources of CO_2 in the global coastal ocean using a spatially-explicit typology of estuaries and continental shelves. Geophys Res Lett. 37:1

Laruelle GG, Lauerwald R, Rotschi J, Raymond P, Hartmann J, Regnier P (2015) Seasonal response of air-water CO_2 exchange along the land-ocean aquatic continuum of the northeast North American coast. Biogeosciences 12:1447

Lee J-M, Kim G (2006) A simple and rapid method for analyzing radon in coastal and ground waters using a radon-in-air monitor. J Environ Radioact 89:219–228

Macklin PA, Maher DT, Santos IR (2014) Estuarine canal estate waters: Hotspots of CO_2 outgassing driven by enhanced groundwater discharge? Mar Chem. 167:82–92

Maher DT, Santos IR, Golsby-Smith L, Gleeson J, Eyre BD (2013) Groundwater-derived dissolved inorganic and organic carbon exports from a mangrove tidal creek: the missing mangrove carbon sink? Limnol Oceanogr 58:475–488

Maher DT, Cowley K, Santos IR, Macklin P, Eyre BD (2015) Methane and carbon dioxide dynamics in a subtropical estuary over a diel cycle: insights from automated in situ radioactive and stable isotope measurements. Mar Chem 168:69–79

Moore WS (2010) The effect of submarine groundwater discharge on the ocean. Ann Rev Mar Sci 2:59–88

Moore WS, Arnold R (1996) Measurement of 223Ra and 224Ra in coastal waters using a delayed coincidence counter. J Geophys Res 101:1321–1329

O'Connor DJ, Dobbins WE (1956) The mechanics of reaeration in natural streams. J Sanit Eng Div 82:1–30

Peterson RN, Santos IR, Burnett WC (2010) Evaluating groundwater discharge to tidal rivers based on a Rn-222 time-series approach. Estuar Coast Shelf Sci 86:165–178

Pierrot D, Neill C, Sullivan K, Castle R, Wanninkhof R, Lüger H, Johannessen T, Olsen A, Feely RA, Cosca CE (2009) Recommendations for autonomous underway pCO_2 measuring systems and data-reduction routines. Deep Sea Res Part II 56:512–522

Porubsky W, Weston N, Moore W, Ruppel C, Joye S (2014) Dynamics of submarine groundwater discharge and associated fluxes of dissolved nutrients, carbon, and trace gases to the coastal zone (Okatee River estuary, South Carolina). Geochim Cosmochim Acta 131:81–97

Raymond PA, Cole JJ (2001) Gas exchange in rivers and estuaries: choosing a gas transfer velocity. Estuaries Coasts 24:312–317

Regnier P, Friedlingstein P, Ciais P, Mackenzie FT, Gruber N, Janssens IA, Laruelle GG, Lauerwald R, Luyssaert S, Andersson AJ (2013) Anthropogenic perturbation of the carbon fluxes from land to ocean. Nat Geosci 6:597–607

Sadat-Noori M, Maher DT, Santos IR (2015a) Groundwater discharge as a source of dissolved carbon and greenhouse gases in a subtropical estuary. Estuaries Coasts 39:1–18

Sadat-Noori M, Santos IR, Sanders CJ, Sanders LM, Maher DT (2015b) Groundwater discharge into an estuary using spatially distributed radon time series and radium isotopes. J Hydrol 528:703–719

Sadat-Noori M, Santos IR, Tait DR, Maher DT (2016) Fresh meteoric versus recirculated saline groundwater nutrient inputs into a subtropical estuary. Sci Total Environ 566–567:1440–1453

Sadat-Noori M, Santos IR, Tait DR, Reading MJ, Sanders CJ (2017) High porewater exchange in a mangrove-dominated estuary revealed from short-lived radium isotopes. J Hydrol 553:188–198

Santos IR, Eyre BD, Huettel M (2012a) The driving forces of porewater and groundwater flow in permeable coastal sediments: a review. Estuar Coast Shelf Sci 98:1–15

Santos IR, Maher D, Eyre BD (2012b) Coupling automated radon and carbon dioxide measurements in coastal waters. Environ Sci Technol 46:7685–7691

Santos IR, Bryan KR, Pilditch CA, Tait DR (2014) Influence of porewater exchange on nutrient dynamics in two New Zealand estuarine intertidal flats. Mar Chem 167:57–70

Schubert M, Paschke A, Lieberman E, Burnett WC (2012) Air-Water Partitioning of 222Rn and its Dependence on Water Temperature and Salinity. Environ Sci Technol 46:3905

Slomp CP, Van Cappellen P (2004) Nutrient inputs to the coastal ocean through submarine groundwater discharge: controls and potential impact. J Hydrol 295:64–86

St-Jean G (2003) Automated quantitative and isotopic (13C) analysis of dissolved inorganic carbon and dissolved organic carbon in continuous-flow using a total organic carbon analyser. Rapid Commun Mass Spectrom 17:419–428

Sun H, Gao Z, Lu P, Xiu P, Chen L (2017) Evaluation of the net CO_2 uptake in the Canada Basin in the summer of 2008. Acta Oceanol Sin 36:94–100

Tait DR, Maher DT, Macklin PA, Santos IR (2016) Mangrove pore water exchange across a latitudinal gradient. Geophys Res Lett 43:3334–3341

Tait DR, Maher DT, Wong WW, Santos IR, Sadat-noori M, Holloway C, Cook PLM (2017) Greenhouse gas dynamics in a salt-wedge estuary revealed by high resolution cavity ring down spectroscopy observations. Environ Sci Technol 51:13771–13778

Wang ZA, Cai WJ (2004) Carbon dioxide degassing and inorganic carbon export from a marsh-dominated estuary (the Duplin River): a marsh CO_2 pump. Limnol Oceanogr 49:341–354

Wang G, Wang Z, Zhai W, Moore WS, Li Q, Yan X, Qi D, Jiang Y (2015) Net subterranean estuarine export fluxes of dissolved inorganic C, N, P, Si, and total alkalinity into the Jiulong River estuary, China. Geochim Cosmochim Acta 149:103–114

Wang SR, Di Iorio D, Cai WJ, Hopkinson CS (2018) Inorganic carbon and oxygen dynamics in a marsh-dominated estuary. Limnol Oceanogr 63:47–71

Wanninkhof R (1992) Relationship between wind speed and gas exchange. Journal of Geophysical Research: Oceans 97:7373–7382

Weiss RF (1974) Carbon dioxide in water and seawater: the solubility of a non-ideal gas. Mar Chem 2:203–215

Weiss R, Price B (1980) Nitrous oxide solubility in water and seawater. Mar Chem 8:347–359

Weston NB, Neubauer SC, Velinsky DJ, Vile MA (2014) Net ecosystem carbon exchange and the greenhouse gas balance of tidal marshes along an estuarine salinity gradient. Biogeochemistry 120:163–189